The effect of beam width and crack-depth ratio on mode I fracture toughness of RCB: an experimental and numerical study

Seleem S. E. Ahmad
Engineering Materials Dept., Faculty of Engineering, Zagazig University, Egypt
seleemahmad62@yahoo.com, http://orcid.org/0000-0001-9894-0209

Ghada M.A. Gamiaa
Engineering Materials Dept., Faculty of Engineering, Zagazig University, Egypt
engineergh49@yahoo.com, https://orcid.org/0009-0004-6290-2330

Abd El-Monem I. El-Kholy
Engineering Materials Dept., Faculty of Engineering, Zagazig University, Egypt
str.eng.elkholy@gmail.com, https://orcid.org/0000-0003-4247-2041

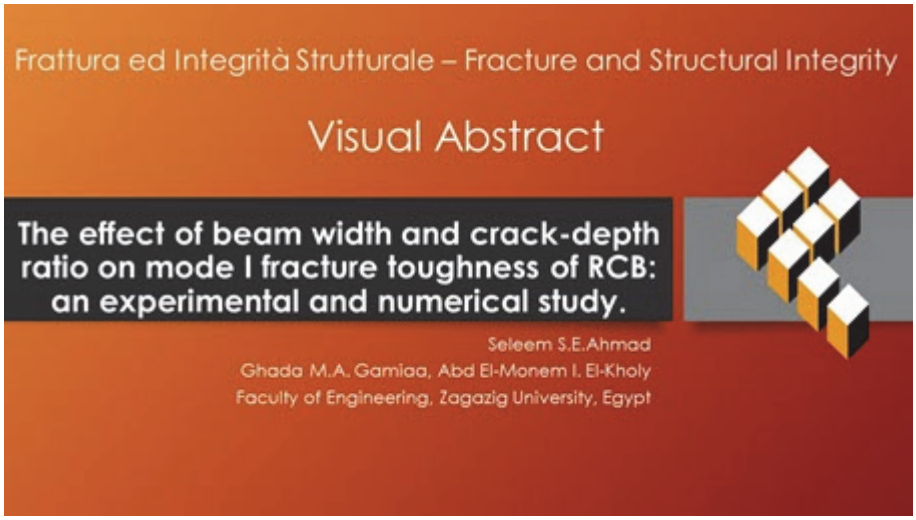

Citation: Ahmad, S. S. E., Gamiaa, G.M.A., El-Kholy, A. I., The effect of beam width, crack-depth ratio and concrete strength on mode I facture toughness of reinforced concrete beams, Frattura ed Integrità Strutturale, 67 (2024) 24-42.

Received: 31.07.2023
Accepted: 05.10.2023
Online first: 28.10.2023
Published: 01.01.2024

KEYWORDS: Fracture toughness, Plain strain $K_{IC,}$ 3-D ANSYS, Mode I crack, Crack to depth ratio, Minimum area of reinforcing.

INTRODUCTION

The process of fracturing in reinforced concrete structures is complex and involves the existence of both short cracks and long cracks. This behavior was influenced by different factors, such as the process zone ahead of the crack tip and crack closing of steel bars, and is dependent on the heterogeneity of the concrete, as well as the type and properties of the reinforcement. Linear elastic mechanics concept through K_{1C} is a valuable and precise method for

estimating the fracture toughness of concrete. By conducting tests on cracked beams, it becomes possible to compute the K_{1C}, which is the critical stress intensity factor for Mode I opening. Nevertheless, it has been established that the value of K_{1C}, as calculated from the maximum load and initial notch length, is subject to the dimensions of the beams.

A study conducted on RCB without transverse reinforcement on the shear was presented in [1]. The study observed the impact of the relative span to effective depth ratio, with a/d values of 2, 1.5, and 1 as the variable parameter. Results showed that the maximum load increased as the relative span to effective depth ratio decreased. As the load increased, the crack width also increased and propagated to the test sample's top surface. The crack opening width's limit values were set at 71-84% of the samples' load-carrying capacity. The increase in shear strength had a similar impact on maximum load and was close in value according to serviceability. A study was conducted using 16 specimens of high-strength RCB [2]. All specimens were the same size but had different initial crack lengths, ranging from 40 mm to 100 mm, and were tested using a three-point bending beam. Based on the results, it is evident that high-strength reinforced concrete has distinct fracture characteristics when compared to normal concrete. The study found that high-strength reinforced concrete's initiation toughness and unstable toughness generally increase with the a/d. Moreover, the initial load to maximum load ratios vary depending on the initial crack length. The ductility of high-strength reinforced concrete is higher when the a/d is bigger, and the ratio is lower.

The use of the digital image technique was explored to analyze crack propagation in RC [3]. Images are captured at various stages of loading, and by comparing these images, one can determine the deformation of an object under external stress. The study focused on the relationship between fracture properties and concrete and steel reinforcement properties. Small-scale reinforced concrete samples were subjected to three-point bending tests, and the technique was used to visualize and quantify the fracture properties. The technique was found to be effective in measuring crack opening displacements. The authors in [4] delve into Carpinteri's previous research on the effect of aggregate materials in fracture tests to explore the effect of the notch in concrete with reinforcing bars. Their experiment found a correlation between the brittleness number and the axial tension force on the reinforcement bar. This allowed them to determine critical values of brittleness number for varying relative crack lengths and ratios of tension force to load at the cracking point. The results demonstrate that utilizing the brittleness number for notch sensitivity analysis is suitable for reinforced concrete beams to determine fracture parameters in fracture tests.

Concrete is made stronger and more durable by adding fibers to the mixture [5-7]. A work conducted by Ali et al. [8] studied the effect of different a/d, and various fiber lengths and a hybrid fiber consisting of 50% of each length for fiber-reinforced concrete, FRC, on K_{IC}. The results showed that increasing a/d reduced the K_{IC} of FRC. Longer debonding fibers had a negative effect on K_{IC}, but the beam with longer fibers had higher fracture energy than the one with shorter fibers. However, increasing fiber length decreased K_{IC} due to an increase in debonding length, which subsequently decreased their efficiency. An experimental study was conducted by El-Emam et al. [9] to evaluate the value of the K_{IC} of FRC. The work included seventeen groups of beams, each with a depth of 150 mm, width of 200 mm, and length of 500 mm. All beams had an a/d of 0.3 and were tested over a span of 400 mm. Using fibers resulted in a higher peak load and energy and a remarkable impact on the stress intensity factor.

The 3-point bending test is considered one of the most widely used methods to investigate a material's fracture properties. [10]. The semicircular bend, single-edge-notched, edge-notched disc, four-point bending, and directional tension specimens were also reported [11-15]. Due to its simplicity and strong theoretical foundation, the three-point bending beam test is a useful and practical method for examining the mechanism behind the fracture phenomenon [16]. Researchers have suggested that reflective cracks are primarily a result of a combination of Mode I and Mode II fracture, or Mixed-Mode fracture under the applied stress that the three-point bending beam test is appropriate for evaluating fractures.

A study conducted by Daneshfar, M., and Hassani [17] investigated the effect of adding short fibers to concrete. They conducted experiments to analyze the effects of specimen dimensions on synthetic FRC. They calculated the changes in fracture energy by producing and testing various concrete beams of different thicknesses and widths under mode I and found that an increase in the thickness and width of the beams resulted in an improvement in fracture toughness and fracture energy. Additionally, when the thickness and width of the beams were increased, the K_{1C} was increased. In a research conducted by Chao Zang [18], pre-notched beam tests tested the fracture properties of asphalt concrete reinforced by basalt fiber. The double-parameter fracture mode I was used to evaluate the fracture behavior of BFRAC. The study found that increasing fiber content significantly improved BFRAC's fracture resistance. Another study analyzed RCB with negative Poisson's ratio and spiral grooves, effectively controlling crack width and having greater residual strength. The study proved that the increase in the HSHT steel bars' reinforcement ratio enhanced the peak load value [19].

A number of studies have been conducted to examine different factors that affect the fracture toughness of composite materials. Fayed et al. [20] investigated the effect of mode II on the mixed-mode fracture stress intensity factor of steel fiber-reinforced concrete. Similarly, Arikan et al. [21] examined the effects of volume fraction and a/d on particle-filled

polymer composite beams reinforced with textile glass fiber. Carpinteri et al. [22] investigated the effect of the water-to-cement ratio on K_{1C} in FRC, while Zhang et al. [23] explored a new type of composite material using steel FRC and examined its mixed-mode properties, while El-Sagheer et al. [24] evaluated K_{IC} numerically for FRC beams. . Lastly, the failure mechanism of the kaolinitic refractory bricks used in lining furnaces and kilns was experientally investigated [25].

Numerical idealization of smooth and cracked reinforced concrete RC beams is a process of representing the behavior of these beams using mathematical models and simulation techniques. This is typically done using finite element analysis or similar numerical methods. The aim is to predict how cracked RC beams will behave under various loads and conditions, taking into account the nonlinear and complex behavior of concrete cracking and steel reinforcement yielding. Several works introduced linear and nonlinear analysis for the behavior of RC beams to show the impact of static and cyclic loading on the mechanical behavior of RC beams [26-29].

In a study conducted by [30], both experimental and non-local finite element analysis techniques were employed to investigate the impact of testing temperature on the mechanical characteristics and crack propagation in refractory cement bricks. The experimental findings revealed that as the testing temperature increases, the thermomechanical behavior of refractory concrete exhibits a critical temperature point at 800 °C, where the compression and tensile strengths reach their maximum values. On the other hand, the numerical simulation results identified two distinct modes of crack propagation. Continuous crack failures were observed when the temperature ranged from 25 to 800 °C, while multi-identified cracks were found to generate a localized damage zone at 1000 °C. The results from [30] demonstrate that the enhanced non-local damage model employed in the study provides a realistic representation of the experimental failure mechanisms.

Ren H. et al. [31] used the discrete element method to investigate the damage evolution process and the effect of maximum aggregate size on the tensile strength of concrete in flattened Brazilian tests. The study established numerical models of flattened Brazilian disks with different aggregate sizes, including 5-10, 5-16, and 5-20 mm, and conducted numerical simulations. While, Yue JG et al [32] used an acoustic emission method to monitor fracture in concrete. They tested 12 specimens with varying strengths using three-point bending tests. The technique identified fracture mode, micro-cracks, and strain energy release. An empirical expression was developed using strain test data and monitored acoustic emission energy data. The researchers in [33] used three-dimensional finite element analyses to study the collapse of Daikai station during the 1995 Kobe earthquake. Separate models were created for the concrete and steel rebars, which were then assembled in a soil-tunnel model. Bilinear models were used for the concrete and steel rebars, and a three-dimensional finite element nonlinear hysteretic model was used for the soil. The simulations accurately reproduced the structural collapse and surface settlement. An adaptive hierarchical multiscale approach for modeling the trans-scale damage evolution in concrete is given in [34]. The problem domain represented by an adaptive hierarchical multiscale finite element model is decomposed into two regions: the macroscopic elastic region and the multiscale critical region prone to damage. The numerical simulations demonstrate that the presented approach can track and quantify concrete trans-scale damage evolution.

This work aimed to investigate experimentally and numerically the fracture performance of pre-cracked reinforced concrete beams. The main focus was to analyze the impact of beam width (b), 120 and 250 mm, and crack-to-depth ratio (a/d) - 0.1, 0.2, and 0.3 on stress intensity factor and fracture energy for reinforced concrete beams, RCB. Both numerical and experimental three-point loading conditions were used. 3-D finite element analysis was conducted using the ANSYS program. Our work attempted to estimate K_{1C} for pre-cracked RC beams using the concept of localized damage as a simple phenomenon.. We did not consider the softening part of the stress-strain response since it was considered a minor portion of the total fracture energy due to the presence of reinforcing steel bars.

Beam Code.	Description, a/d	Beam width, b, mm	Tensile reinforcement
C1	Control, $a/d = 0$	120	2ϕ12mm
C1d1	0.1	120	2ϕ12mm
C1d2	0.2	120	2ϕ12mm
C1d3	0.3	120	2ϕ12mm
C2	Control, $a/d = 0$	250	4ϕ12mm
C2d1	0.1	250	4ϕ12mm
C2d2	0.2	250	4ϕ12mm
C2d3	0.3	250	4ϕ12mm

Table 1: Configurations of test specimens

1.

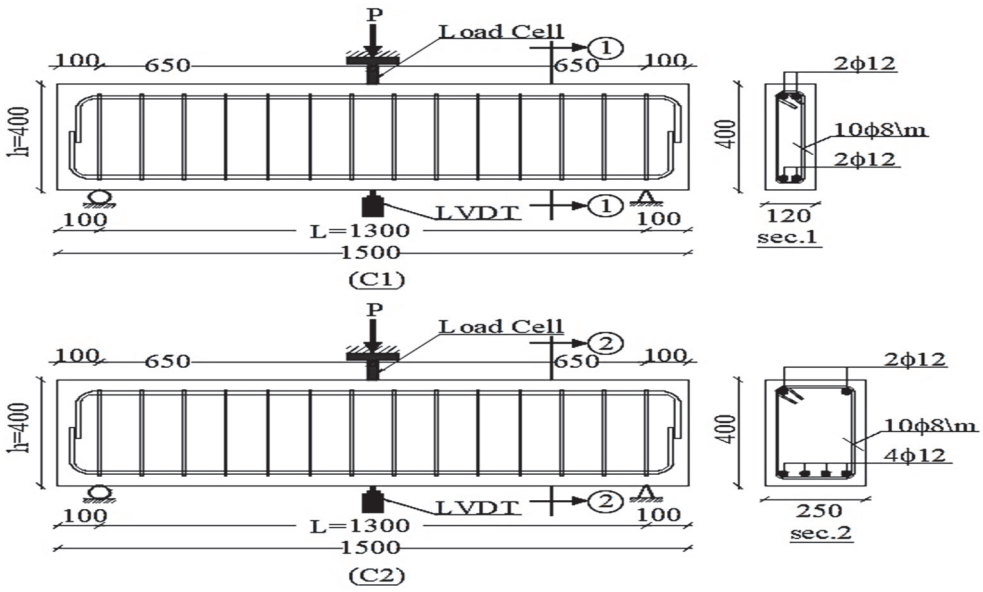

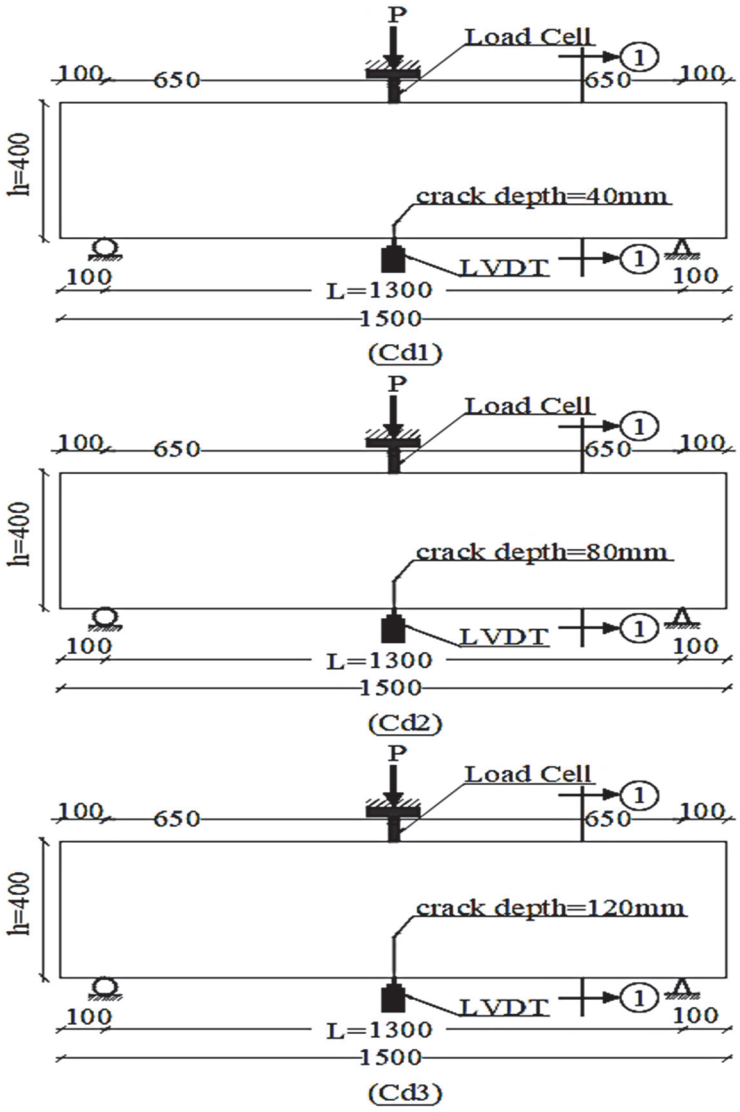

Figure 1: Schemes of experimental specimens.

EXPERIMENTAL PROGRAM

Tab 1 presents the experimental program to investigate the K_{1C} with different beam widths, *b*, and crack depth ratios, *a*/*d*. Fig. 1 shows the schemes dimensions for beams where dimensions are in mm.

A three-point bending test was used. The test included 8 beams, of which 2 were control beams without any cracks. The remaining six beams had different *a*/*d* of 0.1, 0.2, and 0.3. The beams were tested after being cured for around 28 days. The experimental program was categorized into two groups based on the beam dimensions. The first group included beams with dimensions of 120 mm x 400 mm x 1500 mm, while the second group had dimensions of 250 mm x 400 mm x 1500 mm, as shown in Tab. 1.

MATERIAL PROPERTIES

An examination was conducted on the qualities of the used materials, concrete (compressive strength of the tested concrete samples was 40 MPa) and steel (main steel Grad 450 and confinement steel Grad 240). The properties of the concrete were thoroughly tested and analyzed. During the casting of each beam, three cubic concrete samples were taken and subjected to the same curing condition of the beam. At 28 days, they were subjected to a compression test using the ESS of 1658-6/2018 and BS EN 12390/2009, as shown in Fig. 2. Three concrete cylinders with 150 mm diameter and 300 mm height were cast and tested, as shown in Fig. 3. The compressive strength of the tested concrete samples was 40 MPa, while the tensile strength was 2.5 MPa. The reinforcement steel bars were also tested using ESS 262-2/2015 and ISO 6935-2/2007, as shown in Fig. 4. Three specimens were tested for each diameter, and the average results are given in Tab. 2.

Steel.	Yield, MPa	UTS, MPa	% Maximum elongation
Main steel, Grade 450	450	650	18
Confinement steel, Grade 240	240	350	21

Table 2: Mechanical Properties of used steel reinforcement bars.

TEST PROCEDURE

In order to assess the beams' strength, we utilized a universal testing machine that can handle up to 1000 kN and has a calibration error of only 0.4%. The load was applied with a loading rate of 0.7 N/sq mm/min and supported the beams with two rollers. The load was applied at a single point located in the center of the support points, and the mid-span deflection of the beam was measured using linear vertical displacement transducers (LVDT).

Figure 2: Compression test.

Figure 3: Indirect tensile test.

Figure 4: Tension test for reinforcing steel.

To ensure that any cracks would be easily visible, we painted all of the beams white and observed the propagation of any cracks with our naked eyes. Throughout the testing, we utilized a load control system and employed a data logger system that recorded the load-displacement values during the loading process, as shown in Fig. 5.

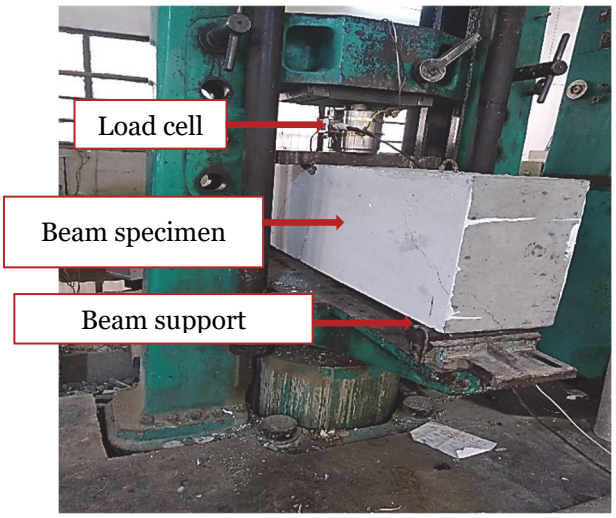

Figure 5: Test setup.

NUMERICAL IDEALIZATION

ANSYS program was used to predict the stress intensity factor for reinforced concrete beams. The numerical idealization depends on the smeared crack approach. This computational technique is widely utilized in structural analysis to simulate the behavior of cracks within materials. Instead of explicitly modeling individual cracks, this approach distributes the effects of cracking throughout the material, offering a computationally efficient way to predict crack propagation and its influence on overall structural response. By incorporating fracture mechanics principles, the smeared crack approach enables engineers and researchers to analyze the effects of cracks on stiffness, strength, and energy dissipation in various materials and structures. While it simplifies complex crack interactions, it may sacrifice the accuracy of capturing fine-scale crack patterns. Despite this trade-off, the smeared crack approach remains a valuable tool for conducting large-scale fracture analyses and optimizing designs [35]. The selecting e elements types, contact details, the used material models, and selecting the analysis type, which considered the displacement control type. A solid element named SOLID 65 was suitable for modeling concrete properties, the element configurations were given in [31], while REINF 264 element was used for modeling reinforcement steel.

A multilinear isotropic hardening model was used for simulating concrete. The stress-strain behavior in compression was used to simulate the concrete plasticity based on Eqns. 1 and 2 [36]. The concrete material properties are given in Tab. 3, where μ is Poisson's ratio

$$f = \frac{E_c \varepsilon}{1 + \left(\frac{\varepsilon}{\varepsilon_0} \right)^2} \tag{1}$$

$$\varepsilon_0 = \frac{2 f_c^{'}}{E_c} \tag{2}$$

where E_c is the initial stiffness, ε is the corresponding strain, and ε_0 is the failure strain

f_{cu}	f_t	E	μ
40 MPa	2.5 MPa	28 GPa	0.2

Table 3: Mechanical properties of concrete

The stress-strain response of concrete in tension is similar to the SOLID 65 cracking model [31].

This study utilized a numerical model and cross-checked experimental data. Specifically, the experimental control beam results were compared with numerical results for a beam with a crack depth of 80 mm and a beam width of 250 mm, as illustrated in Fig. 6. To further validate the steel stress results at 200 kN, element sizes of 20 mm, 30 mm, and 40 mm were employed for sensitivity analysis. The results from the developed numerical model, as depicted in Figs. 6.a and 6.b, demonstrate that the mesh element size of 40 mm is well-suited for simulating the problem at hand. The element size in numerical simulations of cracked RC beams directly impacts the results' accuracy. It's crucial to strike a balance between accurately capturing local behavior (using smaller elements) and managing computational resources efficiently. Conducting sensitivity analyses and comparing results with experimental data or validated models can help ensure the reliability of the numerical simulations, as shown in Fig. 6 b. In general, smaller elements lead to a denser mesh, which can more accurately capture localized effects, such as crack propagation. This is particularly important in regions of stress concentration like crack tips and other discontinuities. The experimental specimens were idealized and numerically simulated, as shown in Figs. 7 a and b.

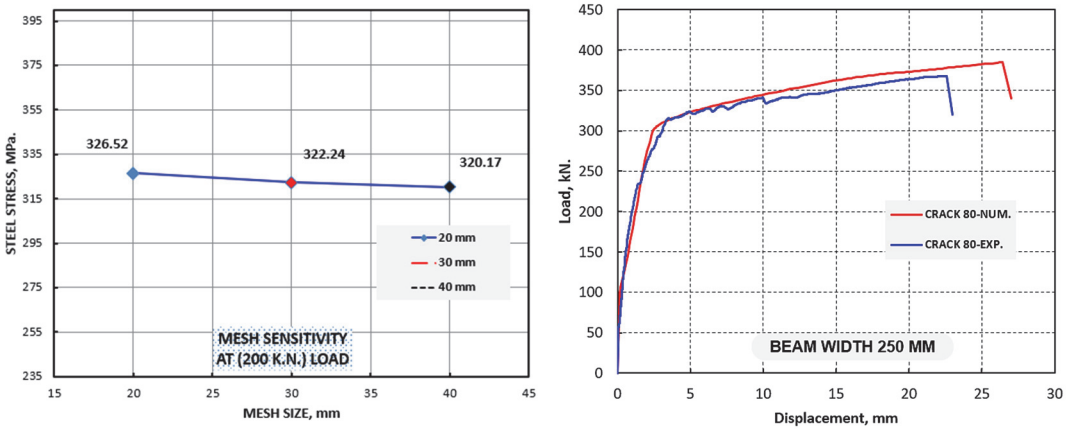

a) Sensitivity to Element Mesh Size. b) Validation of numerical data.

Figure 6: Mesh size sensitivity and validation with experimental data.

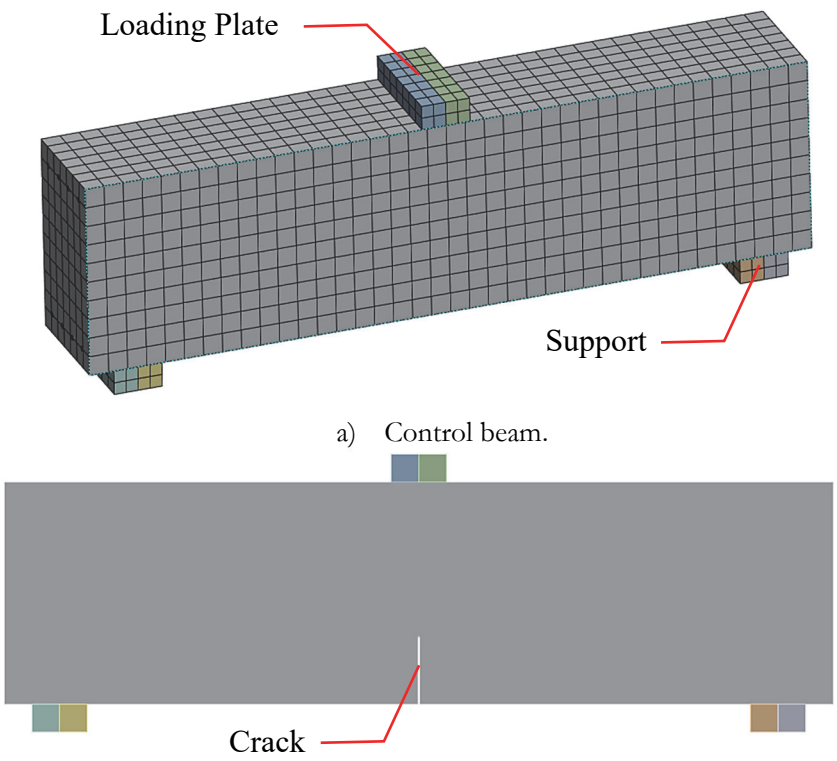

a) Control beam.

b) Beam with developed crack.

Figure 7: Modeling Finite Elements: (a) Beam under Control, (b) Beam with an Advanced Crack.

RESULTS AND DISCUSSION

Experimental results

In Tab. 4, you will find a detailed comparison of experimental results on the b, which can be either 120 mm or 250 mm, and the a/d, which ranges from 0.1 to 0.3. The data for each beam is provided for F_u = 40 MPa. Figs. 8 a and 8 b have been included to show the correlation between applied load and mid-span deflection for control beams and beams with varying a/d at beam widths of 120 mm and 250 mm. The presented figures display the results of the experiment conducted to analyze the impact of the crack depth and beam width ratio on the beam toughness. The acquired data was then used to determine each beam's energy release rate. Usually, to determine the work done to failure and toughness of a tested beam, we calculate the area under the load-deflection curve. We subtract the toughness of the cracked specimen from that of the control specimen without any cracks to calculate the energy release, ΔU. This takes into account the work done for the cracked portion in the cracked specimen. In order to determine the energy release rate, ΔG, we need to divide the ΔU by the area that is cracked, ΔA. Once we have that information, we can calculate the critical stress intensity factor, K_{IC}, using Eqn. 3.

$$K_{IC} = \sqrt{\Delta G\, E} \tag{3}$$

where E is the flexural stiffness and calculated from the load-deflection curve for each beam

The Eqn. (3) used in this study based on the fundamentals of fracture mechanics. It predicts the Mode I stress intensity factor by considering the energy release rate of the cracked area and material stiffness in the global direction. Additionally, the stress intensity factor simplifies the complex stress field and damage near the crack tip by characterizing it with a single parameter [37, 38].

The traditional models, like K_{IC}, only consider the global strain or stress components. However, other models of damage, like the micro plane model, take into account the response at different orientations or micro planes within the material. Adopting such an approach provides a more accurate representation of the anisotropic and heterogeneous nature of damage

and softening in plain concrete and other brittle and heterogeneous materials. Nevertheless, the micro plane model needs to be updated to capture the effect of steel reinforcing bars in RC elements.[39-41].

Fig. 9 gives the behavior of K_{1C}, where K_{1C} increases as the a/d ratio increases, similar to the results found in the literature [3, 4]. Furthermore, the value of K_{1C} increases as the b expands, as found in [17]. The load-deflection curves depicted in Figs. 8 a and 8 b provide invaluable insights into the impact of the crack depth ratio and beam width on beam toughness. As an illustration, if a beam has a width of 120 mm and the a/d increases from 0.1 to 0.2, the K_{1C} increases at a rate of about 0.98%. However, once the a/d surpasses 0.2, the K_{1C} significantly increases. For instance, when the a/d increases from 0.2 to 0.3, K_{1C} increases by approximately 39.22%. The percentage of increasing K_{1C} values are 46 % and 84.67% as the a/d increases from 0.1 to 0.2 and from 0.2 to 0.3, respectively, for a beam width of 250 mm.

The crack patterns and failure modes for the control beam and pre-cracked beams with different a/d of 0.1, 0.2, and 0.3, respectively, are shown in Figs. 10 and 11 a, b, c, and d. For beams with a width of 120 mm, the control beam initially failed by tension cracks, followed by concrete compression failure. On the other hand, the pre-cracked beams failed due to tension cracks, with the cracks in the beam with a crack depth ratio of 0.3 being less in number and wider compared to other pre-cracked beams. A similar trend was observed in the case of beams with a width of 250 mm.

When the a/d increases in plain concrete beams, the number of cracks generated by a head and surrounding main crack decreases. This behavior results in a significant decrease in the fracture resistance and toughness of concrete, which has been confirmed by previous studies such as [42-44]. However, in reinforced concrete beams, the existence of reinforcing steel bars increases the closing effect due to the compressive force generated by the steel bars. This effect becomes more evident as the ratio of crack to depth increases. Therefore, two opposite effects are present in RC beams, and they ultimately control the final value of fracture toughness of reinforced concrete members, which shows an increase in the present study.

Based on the experimental results described, it can be observed that the cracked RC beams exhibited lower maximum loading values and higher maximum deflection values compared to the smooth beams. This behavior resulted in an increase in the total fracture toughness of the cracked beams as the a/d increased. The increase in fracture toughness can be attributed to the development of microcracks ahead of the main crack tip due to stress concentration in the crack process zone during loading.

Additionally, as shown in Tab. 5, the values of the first cracking loads decreased as the a/d increased. This means that the beams with higher crack depth ratios exhibited cracking at lower applied loads. For example, with a beam width of 120 mm, the initial crack load decreased from 38 kN for the smooth beam to 27 kN, 21 kN, and 15 kN for a/d ratios of 0.1, 0.2, and 0.3, respectively. Similar behavior was observed for beams with a width of 250 mm, where the initial crack load decreased as the a/d increased. For example, the initial crack load decreased from 130 kN for the smooth beam to 118 kN, 90 kN, and 72 kN for a/d ratios of 0.1, 0.2, and 0.3, respectively.

The crack patterns observed in the experimental tests indicated that the damage zone area and the number of cracks decreased as the crack depth ratio increased. This decrease in the damage zone and crack formation can be attributed to the stress concentration that occurs when the crack depth ratio increases. Furthermore, this behavior was also observed when the beam width increased, indicating that the crack depth ratio and beam width both influenced the fracture toughness and crack development of the RC beams. Fig. 10 and Fig. 11 likely illustrate the crack patterns and their evolution as the a/d and beam width changed during the experimental tests. Overall, these findings are crucial for understanding the fracture behavior of RC beams with varying crack depth ratios and beam widths, which can aid in designing more robust and safe structures.

Compressive strength, F_{cu} (MPa)	F_{cu} =40					
Thickness (mm)		b=120			b=250	
a/d	0.1	0.2	0.3	0.1	0.2	0.3
Energy release rate, ΔG (kN.mm)	3187	3939	4282	6460	7370	8398
Stress intensity factor, K_{1C} ($kN.mm^{-1.5}$)	102	103	142	150	219	277

Table 4: Experimental results.

Thickness (mm)	b=120				b=250			
a/d	0	0.1	0.2	0.3	0	0.1	0.2	0.3
First crack loading, kN	38	27	21	15	130	118	90	72

Table 5: First crack loading

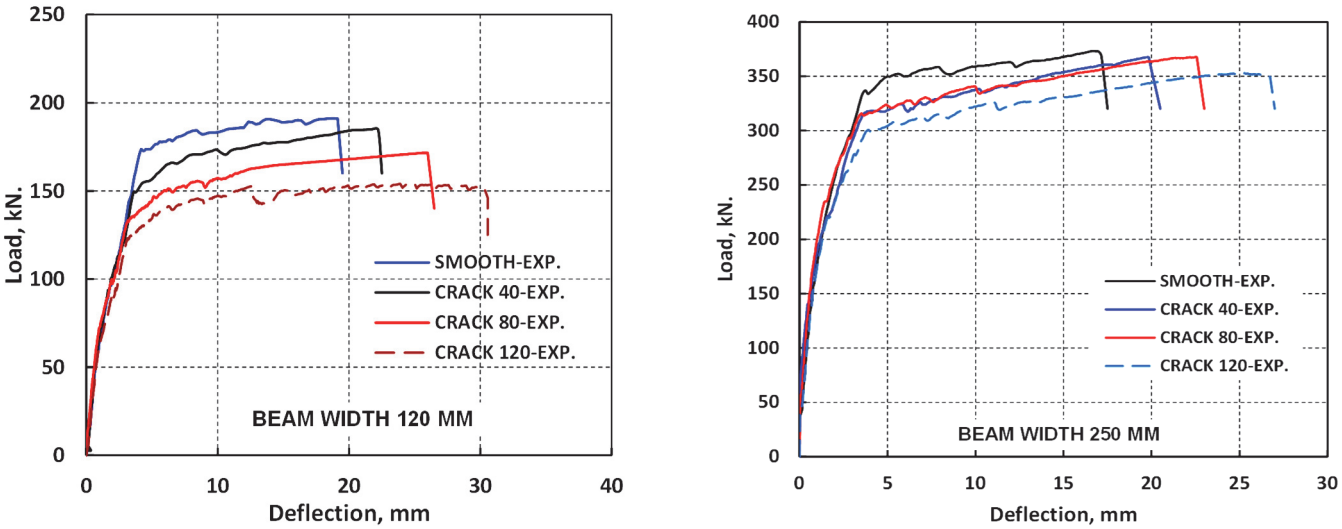

a) beam width 120 mm b) beam width 250 mm

Figure 8: Experimental load-deflection relationship; a) beam width 120 mm b) beam width 250 mm.

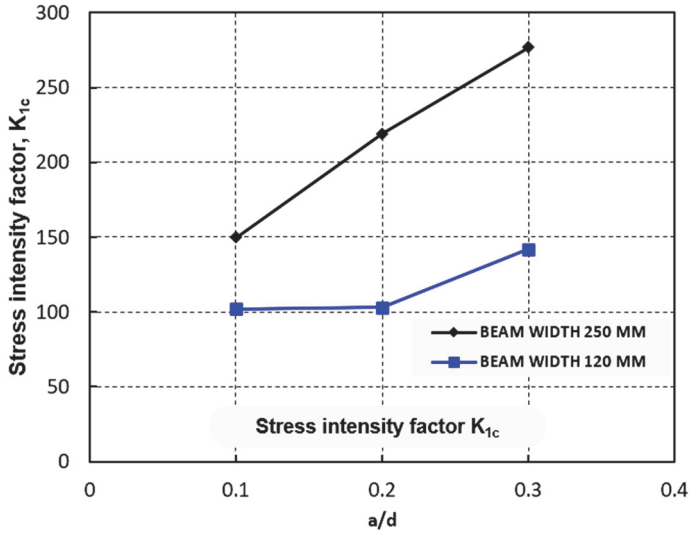

Figure 9: Behavior of K_{1C} against a/d for b = 120 and 250 mm.

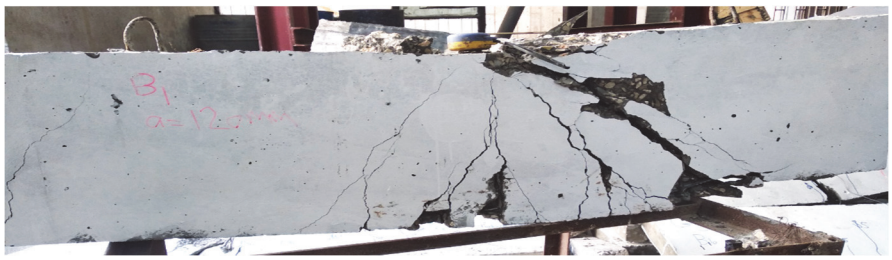

a) control beam, b=120 mm

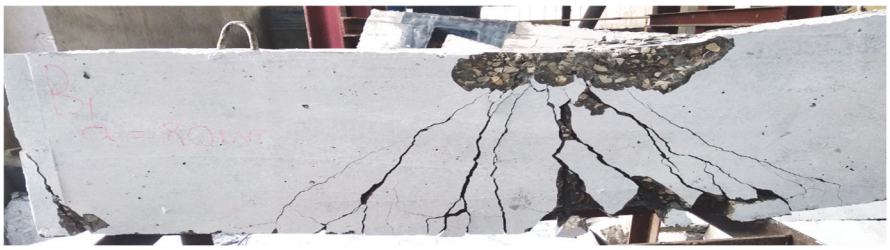

b) a/d = 0.1, b=120 mm

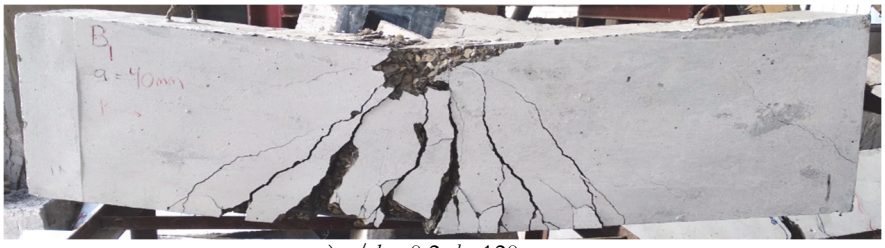

c) a/d = 0.2, b=120 mm

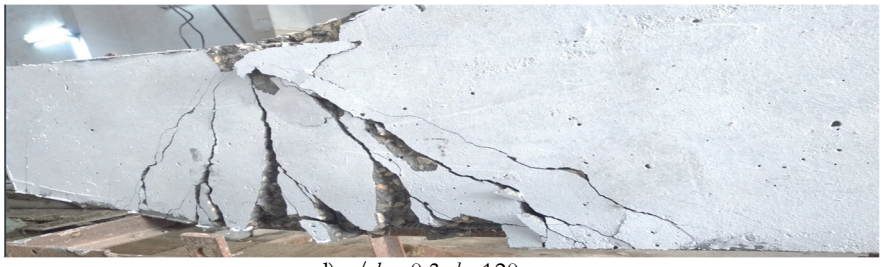

d) a/d = 0.3, b=120 mm

Figure 10: Experimental crack patterns at maximum deflection; beams width 120 mm.

a) control beam, b=250 mm

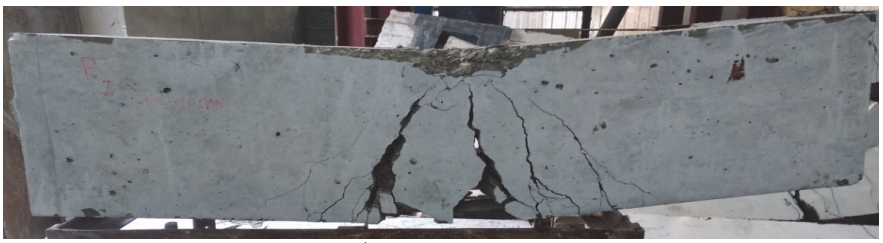

b) a/d = 0.1, b=250 mm

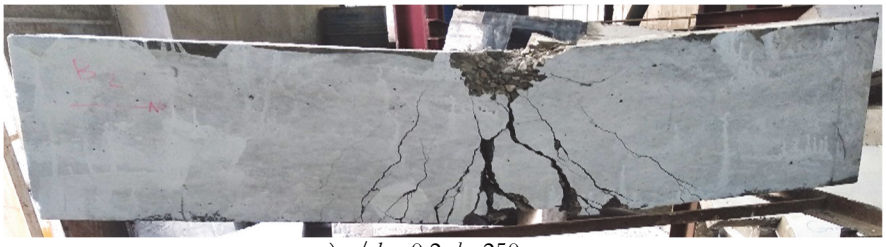

c) a/d = 0.2, b=250 mm

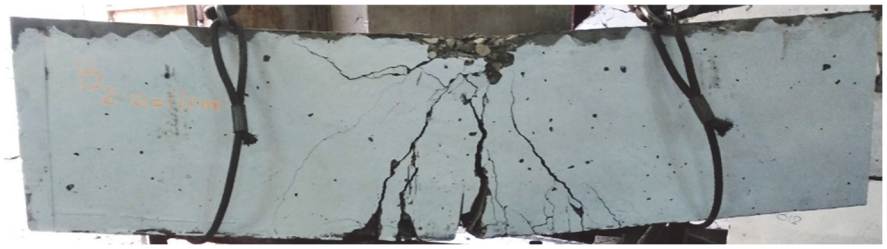

d) a/d = 0.3, b=250 mm

Figure 11: Experimental crack patterns at maximum deflection; beams width 250 mm.

Numerical results

The numerical results for ΔG and K_{1C} are presented in Tab. 6 for comparison between simulated beam widths of 120 or 250 mm and a/d of 0.1, 0.2, or 0.3. The data for each beam is given at a compressive strength of F_{cu} = 40 MPa. Figs. 12 a and 12 b illustrate the numerical relationship between the applied load and mid-span deflection for the control beam and the beam with a/d of 0.1, 0.2, and 0.3 for both beam widths.

Fig. 13 shows the stress intensity factor, K_{1C}. The numerical results indicate that the beam toughness is affected by the a/d and b, as shown by the load-deflection curves. It is important to note that a higher a/d and wider beam width lead to an increase in K_{1C}, as demonstrated by chart references [3, 4, 43].

When the beam width is 120 mm, and the a/d increases from 0.1 to 0.2, the K_{1C} increases by approximately 37.27%. As the a/d increases from 0.2 to 0.3, K_{1C} increases at a slower rate, with an increase of around 38.18%. For a beam width of 250 mm, the percentage increases in K_{1C} values are 53.98% and 134.51% as the a/d increases from 0.1 to 0.2 and from 0.2 to 0.3, respectively. In Figs. 14 and 16, the simulated beams show the crack initiation, while Figs. 15 and 17 show the crack pattern at failure as found by numerical analysis. The width of the crack can be determined by analyzing the values of the crack mouth opening displacement (CMOD). The parameter is essential in understanding the damage process and behavior of the crack and predicting its propagation. Detailed illustrations of the crack width based on this parameter can be found in figures. The data of CMOD suggests that increasing beam thickness (b) at the same a/d ratio leads to a decrease in CMOD, indicating less damage and improved resistance to crack propagation. This finding aligns with the enhanced fracture toughness (K_{IC}) observed in beams with a thickness of 250 mm; thicker beams seem to be more robust against crack formation and propagation, making them a potentially better choice in situations where crack resistance is crucial.

Tab. 7 provides the detailed numerical values for the initial crack loads and the corresponding generated stresses in reinforcing bars for both beam widths (250 mm and 120 mm) and various a/d. Based on the numerical results, it is evident that the initial crack loads decrease as the crack depth ratio (a/d) increases for both beam widths. For the 250 mm width beams, the initial crack loads decrease from 138.39 kN (smooth beam) to 123.40 kN (a/d=0.1), 106.53 kN (a/d=0.2), and 100.38 kN (a/d=0.3). Similarly, for the 120 mm width beams, the initial crack loads decrease from 40.12 kN (smooth beam) to 29.61 kN (a/d=0.1), 23.15 kN (a/d=0.2), and 18.22 kN (a/d=0.3).

The crack patterns observed in the experimental tests indicate that the damage zone area and the number of cracks decrease as the crack depth ratio increases, which can be attributed to the occurrence of stress concentration as the crack depth ratio increases. This phenomenon is also observed when the beam width increases.

These numerical findings provide valuable insights into the fracture behavior of RC beams with varying crack depth ratios and beam widths, which is essential for designing structures that can resist cracking and ensure the safety and performance of RC beams under different loading conditions.

.

Compressive strength, F_{cu} (MPa)	F_{cu} =40					
Thickness(mm)	b=120			b=250		
a/d	0.1	0.2	0.3	0.1	0.2	0.3
Energy release rate, ΔG (kN.mm)	3631	3970	4000	8383	9000	10440
Stress intensity factor, K_{1C} ($kN.mm^{-1.5}$)	110	151	152	113	174	265

Table 6: Numerical results.

Thickness (mm)	*b*=120				*b*=250			
a/*d*	0	0.1	0.2	0.3	0	0.1	0.2	0.3
First crack loading, kN	40.12	29.61	23.15	18.22	138.39	123.40	106.53	100.38
Steel stress at first crack, MPa	70.95	68.49	56.87	55.90	189.05	187.00	104.11	102.71

Table 7: First crack loading and steel stress at first crack.

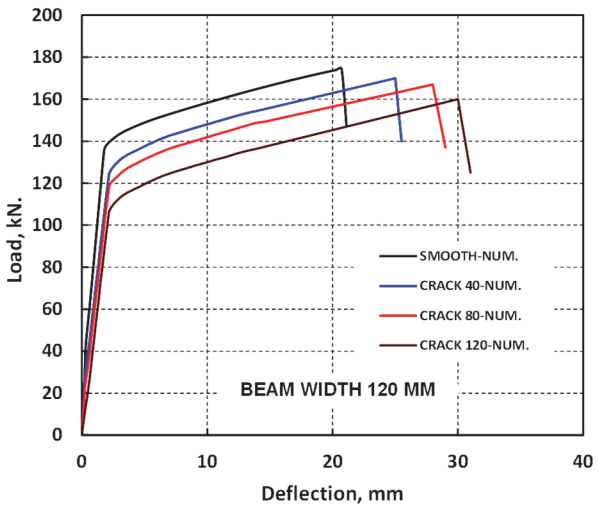

a) beam width 120 mm

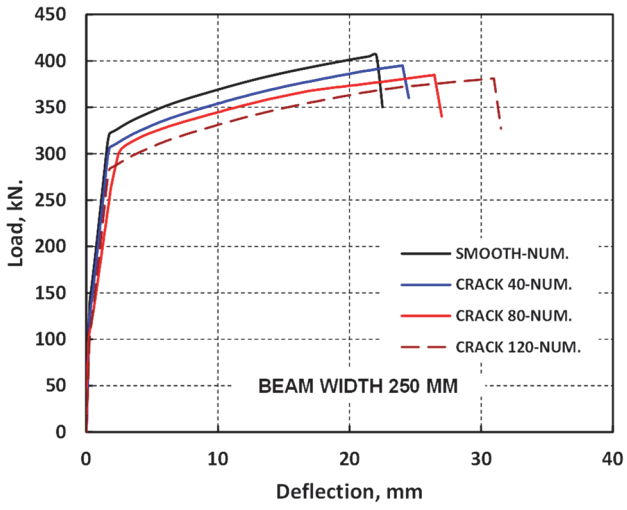

b) beam width 250 mm

Figure 12: Numerical load-deflection relationship; a) beam width 120 mm b) beam width 250 mm.

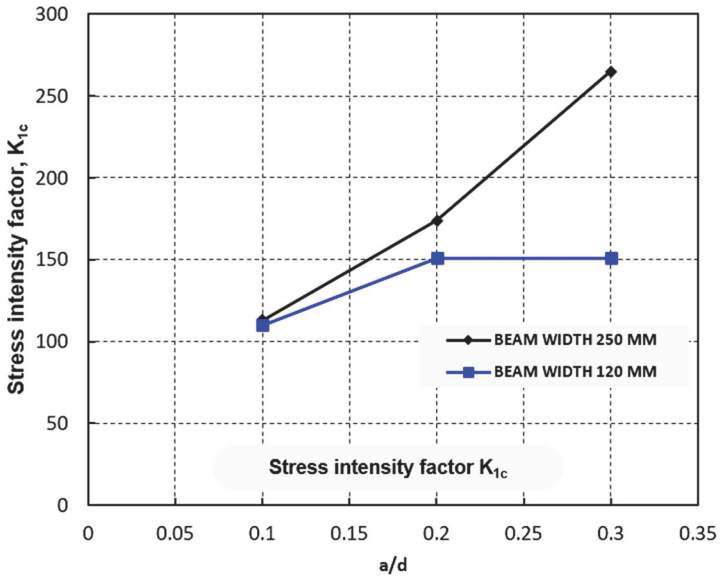

Figure 13: Numerical K_{1C} against *a*/*d* for specimens' width *b* = 120 and 250 mm

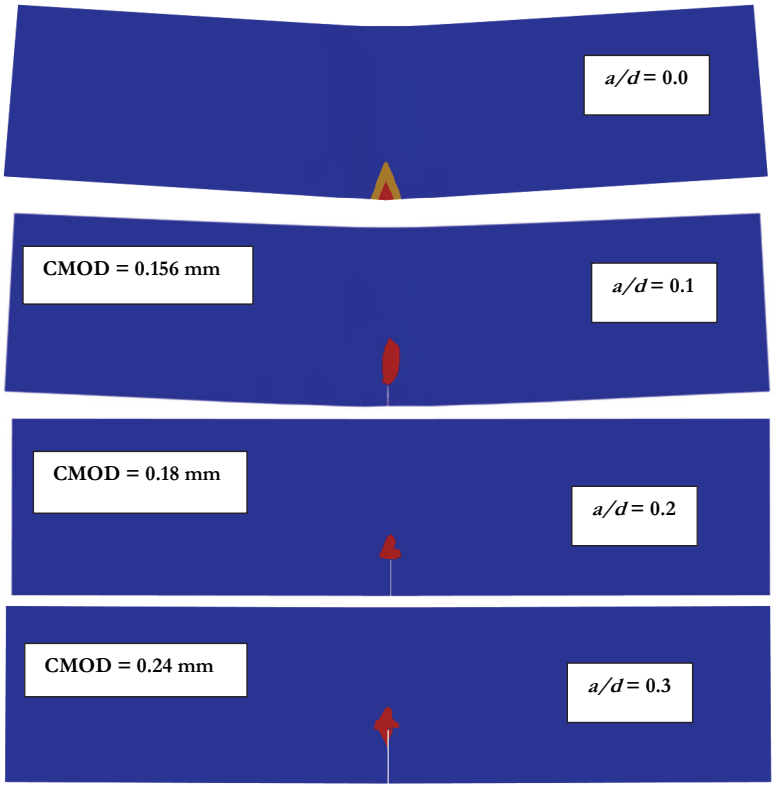

Figure 14: Crack initiation; *b* 120 mm.

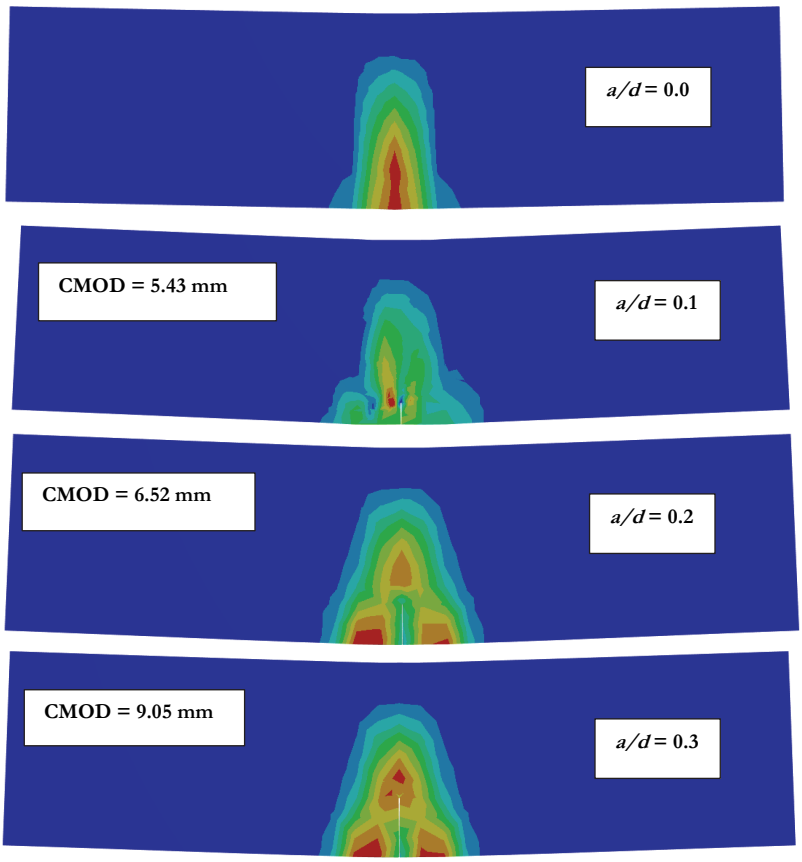

Figure 15: Numerical crack patterns at failure; *b* 120 mm.

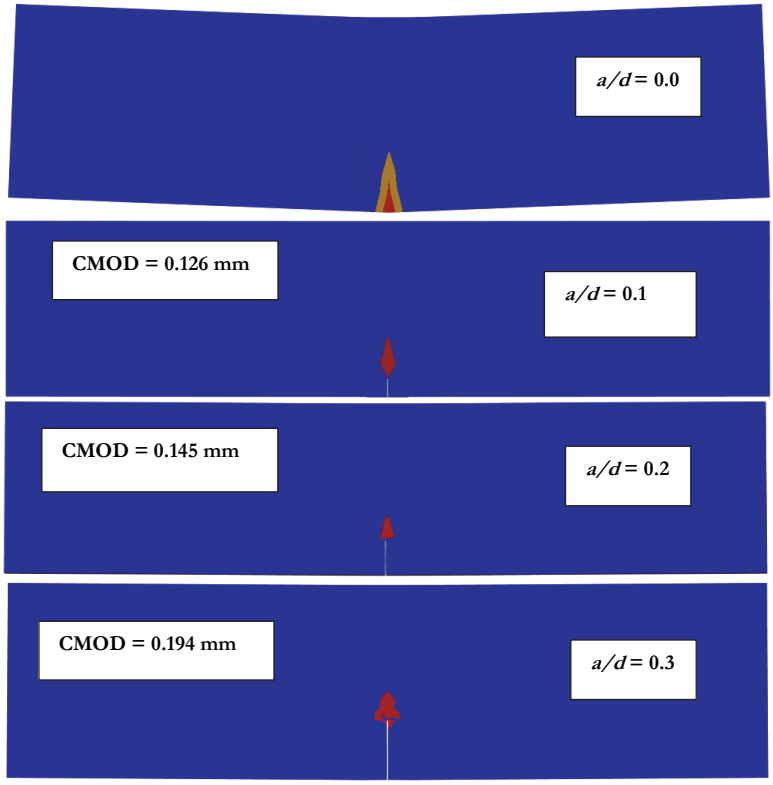

Figure 16: Crack initiation; *b* 250 mm.

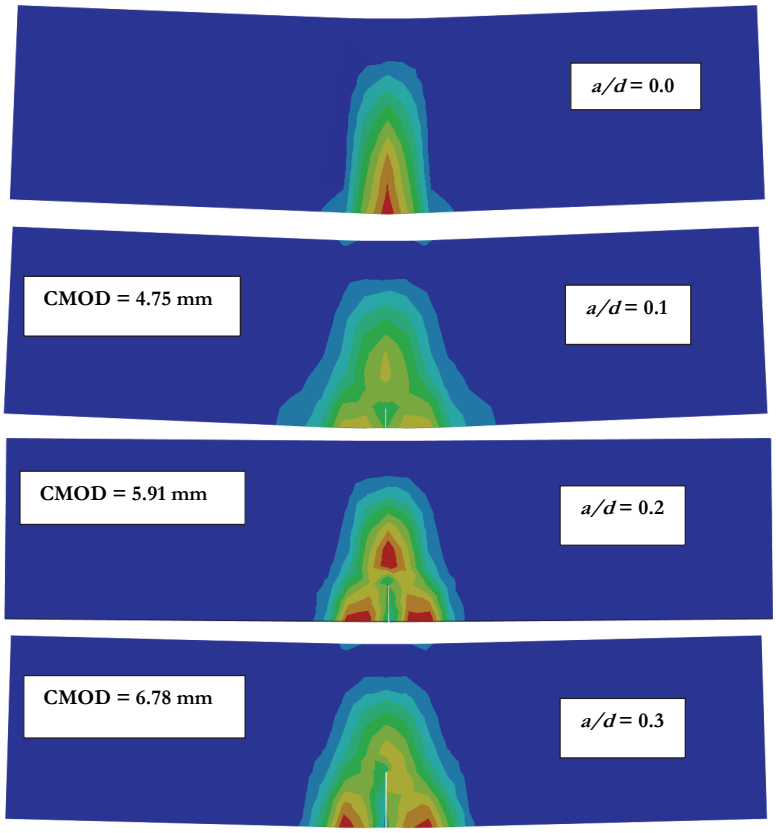

Figure 17: Numerical crack patterns at failure; *b* 250 mm.

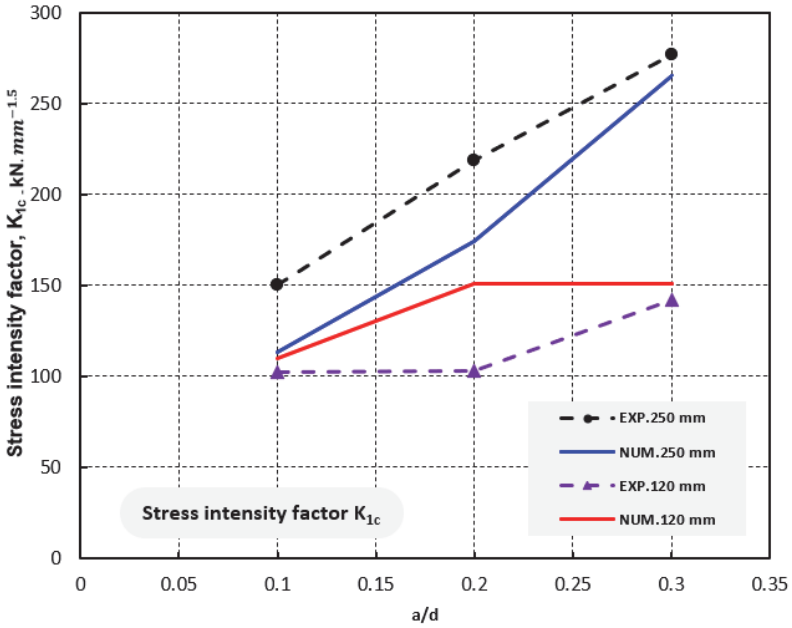

Figure 18: Experimental and numerical K_{1C} against a/d for specimens' width b = 120 and 250 mm.

Comparison between experimental and numerical K_{1c}

Experimental data and numerical methods provide insights into material behavior. Numerical simulations allow for parametric studies of complex scenarios, while experimental testing validates real-world conditions. Combined, these approaches provide a comprehensive understanding of material behavior. In this section, a comparison between the obtained results of experimental and numerical K_{1C} was given. Fig. 18 presents the correlation between a/d and K_{1C} for b values of 120 and 250 mm numerically and experimentally. The results exhibit that the behavior of K_{1C}, both experimentally and numerically, is quite similar. It is observed that with an increase in a/d and b, K_{1C} also increases. In the case where b = 120 mm, the K_{1C} numerical results exceeded the experimental results for all a/d values, with differences of roughly 8%, 45%, and 7% for a/d values of 0.1, 0.2, and 0.3, respectively. On the other hand, in the case where b = 250 mm, K_{1C} numerical results were consistently lower than experimental results for all a/d values. Differences were approximately 24%, 20%, and 4% for a/d values of 0.1, 0.2, and 0.3, respectively. One can notice a remarkable decrease in the difference between experimental and numerical results, especially with increasing in a/d.

Conclusions

This study examined 8 reinforced concrete beams with different crack depths and widths. Both experimental and numerical methods were used. The study found certain conclusions.

1- The K_{1C} is influenced by the width of the specimen. When the beam width is increased from 120 mm to 250 mm, there is an experimental increase of approximately 46% and 84.67% and a numerical increase of about 53.98% and 134.51%.

2- The K_{1C} is affected by the a/d, and it has been observed that an increase in the a/d from 0.1 to 0.2 for a beam width of 120 mm results in a 0.98% and 39.22% increase in the K_{1C}. Similarly, an increase in the a/d from 0.2 to 0.3 for the same beam width results in a 46% and 84.67% increase in K_{1C}.

3- When a crack is present, stress tends to concentrate at its tip, causing a reduction in the total number of cracks that will occur.

4- When the a/d increases, the impact of steel reinforcement also increases due to the increased moment arm from the centroid of the steel to the crack tip.

5- There is a remarkable decrease in the difference between experimental and numerical results, especially with increasing in a/d.

REFERENCES

[1] Vegera, P., Vashkevych, R. , Blikharskyy, Z. (2018). Fracture toughness of RC beams with different shear span. Matec Web of Conferences, 174, 02021. DOI: 10.1051/matecconf/201817402021.

[2] Fan, X., Hu, S. (2013). Influence of crack initiation length on fracture behaviors of reinforced concrete. Applied clay science, 79, pp. 25-29. DOI: 10.1016/j.clay.2013.02.026.

[3] Fayyad, T. M., Lees, J. M . (2014) . Application of digital image correlation to reinforced concrete fracture. Procedia Materials Science, 3, pp.1585-1590. DOI: 10.1016/j.mspro.2014.06.256.

[4] Hu, Y., Wang, J., Zhang, C ., Li, H ., Hu, X . (1993). Notch sensitivity of reinforced concrete in fracture tests. Engineering fracture mechanics, 46, pp. 677- 681. DOI: 10.1016/0013-7944(93)90173-P.

[5] Schnütgen, B., Vandewalle, L . (2003).PRO 31. International RILEM Workshop on Test and Design Methods for Steel Fibre Reinforced Concrete-Background and Experiences. RILEM Publications.

[6] Di Prisco, M ., Felicetti , R ., Plizzari, G. A.(2014). PRO 39. 6th International RILEM Symposium on Fibre-Reinforced Concretes (FRC). 1. RILEM Publications.

[7] Di Prisco, M. (2007). Fibre-reinforced concrete for strong, durable and cost-saving structures and infrastructures. Starrylink.

[8] Ali, A. , El-Emam, H. , Seleem, M. , Sallam, H. , Moawad, M. (2022). Effect of crack and fiber length on mode I fracture toughness of matrix-cracked FRC beams. Construction and Building Materials, 341, 127924. DOI: j.conbuildmat.2022.127924.

[9] Hussien, M ., Moawad, M ., Seleem, M ., Sallam, H ., El-Emam, H . (2022). Mixed-mode fracture toughness of high strength FRC.a realistic experimental approach. Archives of Civil and Mechanical Engineering, 22, 168. DOI: 10.1007/s43452-022-00492-8.

[10] Sun, X ., Gao, Z ., Cao, P., Zhou, C. (2019). Mechanical properties tests and multiscale numerical simulations for basalt fiber reinforced concrete.Construction and building materials, 202, pp. 58-72. DOI:10.1016/j.conbuildmat.2019.01.018

[11] Al-Qadi, I. L., Said, I. M., Ali, U. M., Kaddo, J. R. (2021). Cracking prediction of asphalt concrete using fracture and strength tests. International Journal of Pavement Engineering, pp.1-13. DOI: 10.1080/10298436.2021.1892108.

[12] Lu, D. X., Bui, H. H., Saleh, M. (2021). Effects of specimen size and loading conditions on the fracture behaviour of asphalt concretes in the SCB test. Engineering Fracture Mechanics, 242, 107452. DOI:10.1016/j.engfracmech.2020.1.

[13] Lu, D. X., Saleh, M., and Nguyen, N. H. T. (2020). Evaluation of Fracture and Fatigue Cracking Characterization Ability of Nonstandardized Semicircular-Bending Test for Asphalt Concrete. Journal of Materials in Civil Engineering, 32(8), 04020215. DOI:10.1061/(asce)mt.1943-5533.000329.

[14] Meza-Lopez, J., Noreña, N., Meza, C., Romanel, C. (2020). Modeling of Asphalt Concrete Fracture Tests with the Discrete-Element Method. Journal of Materials in Civil Engineering, 32(8), 04020228. DOI:10.1061/(asce)mt.1943-5533.0003305.

[15] Motamedi, H., Fazaeli, H., Aliha, M. R. M., and Reza Amiri, H. (2020). Evaluation of temperature and loading rate effect on fracture toughness of fiber reinforced asphalt mixture using edge notched disc bend (ENDB) specimen. Construction and Building Materials, 234, 117365. DOI:10.1016/j.conbuildmat.2019.11.

[16] Biligiri, K .P., Said ,S., Hakim, H. (2012). Asphalt Mixtures' Crack Propagation Assessment using Semi-Circular Bending Tests. International Journal of Pavement Research and Technology, 5.

[17] Daneshfar, M., Hassani, A., Aliha, M. R. M., Sadowski, T. (2023). Assessment of the Specimen Size Effect on the Fracture Energy of Macro-Synthetic-Fiber-Reinforced Concrete. Materials, 16, 673. DOI: 10.3390/ma16020673.

[18] Zhang, C., Shi, F., Cao, P., Liu, K . (2022). The fracture toughness analysis on the basalt fiber reinforced asphalt concrete with prenotched three-point bending beam test. Case Studies in Construction Materials, 16, e01079. DOI: 10.1016/j.cscm.2022.e01079.

[19] Zhang, Y., Xiong, X ., Liang, Y., He, M. (2023). Study on flexural behavior of concrete beams reinforced with hybrid high-strength and high-toughness (HSHT) and ordinary steel bars. Engineering Structures, 285, 115978. DOI: 10.1016/j.engstruct.2023.115978.

[20] Fayed, A., Abd-Alhady, A., Sherbini, H., Sallam, H. (2008). Crack path in steel fiber reinforced concrete composite under mixed mode. ASJCE Fac Eng Ain Shams Univ, Cairo, 1, pp.17-26.

[21] Arikan, H. (2012). Fracture behavior of textile glass fiber reinforced polymer concrete according to mixed-mode. Journal of Thermoplastic Composite Materials, 25, pp.663-790. DOI: 10.1177/0892705711412649.

[22] Carpinteri, A., Brighenti, R. (2010). Fracture behaviour of plain and fiber-reinforced concrete with different water content under mixed mode loading. Materials & Design, 31(4), pp. 2032–2042. DOI:10.1016/j.matdes.2009.10.021.

[23] Zhang, H. D., Xu, X. S. (2013). Research on test of fracture toughness and fracture criterion of crack of mixed mode I and II of steel fiber concrete.Advanced Materials Research, 671, pp.1688-1691. DOI: 10.4028/www.scientific.net/AMR.671-674.1688.
[24] El-Sagheer, I., Abd-Elhady, A. A., Sallam, H. E-D. M., Naga, S. A. (2021). An assessment of ASTM E1922 for measuring the translaminar fracture toughness of laminated polymer matrix composite materials. Polymers, 13(18), 3129. DOI: 10.3390/polym13183129.
[25] Mamen, B., Kolli, M., Ouedraogo, E., Hamidouche, M., Djoudi, H., Fanttozi, G. (2018). Experimental characterisation and numerical simulation of the thermomechanical damage behaviour of kaolinitic refractory materials. Journal of the Australian Ceramic Society. DOI:10.1007/s41779-018-0262-8.
[26] Durand, R., Vieira, J., Farias, M. (2023). Numerical analysis of bonded and unbonded prestressed RC beams using cohesive and non-compatible rod elements. Engineering Structures, 288, 116157. DOI: 10.1016/j.engstruct.2023.116157.
[27] Nasrudin, N . N ., Ariffin, N. F., Alias, A ., Hasim, A . M ., Zaimi, M .S. (2022). Experimental validation of reinforced concrete beam incorporating coal fly ash and coal bottom ash using numerical analysis. Engineering Technology International Conference, (ETIC 2022), Online Conference, Kuantan, Malaysia, pp. 458-464. DOI: 10.1049/icp.2022.2661.
[28] Karalar, M. (2020). Experimental and Numerical Investigation on Flexural and Crack Failure of Reinforced Concrete Beams with Bottom Ash and Fly Ash. Iranian Journal of Science and Technology, Transactions of Civil Engineering, 44(S1), pp. 331–354. DOI:10.1007/s40996-020-00465-y.
[29] Godat, A., Chaallal, O., Obaidat, Y. (2020). Non-linear finite-element investigation of the parameters affecting externally-bonded FRP flexural-strengthened RC beams.Results in Engineering, 8, 100168. DOI:10.1016/j.rineng.2020.100168.
[30] Mamen, B ., Benali, F., Boutrid, A ., Sahli, M ., Hamidouche, M ., Fantozzi, G. (2021). Experimental investigation and non-local modelling of the thermomechanical behaviour of refractory concrete. Ceramics–Silikáty; 65(3), pp.295-304. DOI: 10.13168/cs.2021.0031.
[31] Ren, H., Song, S., Ning, J. (2022). Damage evolution of concrete under tensile load using discrete element modeling. Theoretical and Applied Fracture Mechanics, 122, 103622. DOI: 10.1016/j.tafmec.2022.103622.
[32] Yue, J. G., Kunnath, S. K., Xiao, Y. (2020). Uniaxial concrete tension damage evolution using acoustic emission monitoring. Construction and Building Materials, 232, 117281. DOI:10.1016/j.conbuildmat.2019.117281.
[33] Nguyen, V.-Q., Nizamani, Z. A., Park, D., Kwon, O.-S. (2020). Numerical simulation of damage evolution of Daikai station during the 1995 Kobe earthquake. Engineering Structures, 206, 110180. DOI:10.1016/j.engstruct.2020.110180.
[34] Xu, L ., Jiang, L ., Shen, L ., Gan, L ., Dong ,Y ., Su, C. (2023). Adaptive hierarchical multiscale modeling for concrete trans-scale damage evolution.International Journal of Mechanical Sciences, 241, 107955. DOI: 10.1016/j.ijmecsci.2022.107955.
[35] Marzec, I., Bobiński, J., Tejchman, J., Schönnagel, J. (2021). Finite element analysis on failure of reinforced concrete corner in sewage tank under opening bending moment. Engineering Structures, 228, 111506. DOI:10.1016/j.engstruct.2020.111506 .
[36] Pandimani, Ponnada, M . R ., Geddada, Y. (2022). Numerical nonlinear modeling and simulations of high strength reinforced concrete beams using ANSYS. Journal of Building Pathology and Rehabilitation, 7, 22. DOI: 10.1007/s41024-021-00155-w
[37] Albrecht, P., Yamada, K . (1977). Rapid calculation of stress intensity factors. Journal of the Structural Division, 103, pp. 377-389. DOI: 10.1061/JSDEAG.0004556.
[38] Radaj, D. (2013). State-of-the-art review on extended stress intensity factor concepts. Fatigue & Fracture of Engineering Materials & Structures, 37(1), pp.1–28. DOI:10.1111/ffe.12120.
[39] Baznt, Z. P., Ožbolt, J. (1990). Nonlocal Microplane Model for Fracture, Damage, and Size Effect in Structures. Journal of Engineering Mechanics, 116(11), pp. 2485–2505. DOI:10.1061/(asce)0733-9399(1990)116:11(2485) .
[40] Bažant, Z.P., Oh, B.H. (1985). Microplane model for progressive fracture of concrete and rock. Journal of Engineering Mechanics, 111, pp.559-582. DOI: 10.1061/(ASCE)0733-9399(1985)111:4(559)).
[41] Bažant, Z.P., Prat, P.C. (1988). Microplane model for brittle-plastic material: I. Theory. Journal of Engineering Mechanics, 114, pp.1672-1688. DOI: 10.1061/(ASCE)0733-9399(1988)114:10(1672).
[42] Pereira, S.S.R., Carvalho, H., Dias, J.V.F., Mendes, V. R .V., Montenegro, P. A. (2019). Behavior of precast reinforced concrete columns subjected to monotonic short-term loading. Frattura ed Integrità Strutturale, 13, pp.242-250. DOI: 10.3221/IGF-ESIS.50.20.

[43] Kumar, M. K., Gopu, G. N. (2016). Analysis of Fracture Parameters in Concrete by Using ABAQUS Software. International Journal of Scientific Engineering and Research (IJSER), 2, 2320-723X.
[44] ELSayed, S.S., Gamiaa, G. M. A. E., (2020). Numerical Analysis of Mode I Fracture Toughness for Plain Concrete Beams. MEJ-Mansoura Engineering Journal, 44, pp.1-6. DOI: 10.21608/bfemu.2020.95008.